X-Ray Computed Tomography Methods for *In Vivo* Evaluation of Local Drug Release Systems

Kyle A. Salem, *Student Member, IEEE*, Agata Szymanski-Exner, Roee S. Lazebnik, Michael S. Breen, Jinming Gao, and David L. Wilson*, *Member, IEEE*

***Abstract*—Recent advances in drug delivery techniques have necessitated the development of tools for *in vivo* monitoring of drug distributions. Gamma emission imaging and magnetic resonance imaging suffer from problems of resolution and sensitivity, respectively. We propose that the combination of X-ray CT imaging and image analysis techniques provides an excellent method for the evaluation of the transport of platinum-containing drugs from a localized, controlled release source. We correlated local carboplatin concentration with CT intensity, producing a linear relationship with a sensitivity of 62.6 μg/mL per Hounsfield unit. As an example application, we evaluated the differences in drug transport properties between normal and ablated rabbit liver from implanted polymer millirods. The use of three–dimensional visualization provided a method of evaluating the placement of the drug delivery device in relation to the surrounding anatomy, and registration and reformatting allowed the accurate comparison of the sequence of temporal CT volumes acquired over a period of 24 h. Taking averages over radial lines extending away from the center of the implanted millirods and integrating over clinically appropriate regions, yielded information about drug release from the millirod and transport in biological tissues. Comparing implants in normal and ablated tissues, we found that ablation prior to millirod implantation greatly decreased the loss of drug from the immediate area, resulting in a higher average dose to the surrounding tissue. This work shows that X-ray CT imaging is a useful technique for the *in vivo* evaluation of the pharmacokinetics of platinated agents.**

***Index Terms*—Carboplatin, CT imaging, image analysis, image registration, molecular imaging, pharmacokinetics.**

I. Introduction

SITE-SPECIFIC delivery of drugs still remains an elusive goal despite intensive research efforts in both academia and industry. In the last 20 years, traditional research efforts have been mostly focused on a "chemical" targeting strategy, which relies on the molecular recognition of unique surface signatures of target tissues by chemical ligands (e.g., antibody-drug conjugates and immunoliposomes) [1], [2]. Although initial successes were achieved in cell culture experiments *in vitro*, these systems were not successful *in vivo* due to a number of physiological barriers [3]–[5]. Recently, we have developed a "physical" targeting strategy for tumor-specific delivery of drugs. In this technique, a cylindrical controlled release drug delivery device, consisting of platinum-containing anticancer agents entrapped in a biocompatible and biodegradable polymer matrix, is fabricated. Under image guidance, the device can be percutaneously implanted directly into a tumor to provide minimally invasive, site-specific delivery of anticancer drugs. Over time, the active drugs will be released at a controlled rate from the delivery device directly into the surrounding tumor tissue to eliminate cancer cells.

To validate the efficacy of this new technique, or any other localized drug delivery system, it is necessary to understand the pharmacokinetics of the device *in vivo*. Questions regarding the rate and quantity of drug release from the device, dynamics of drug distribution in tumor tissues, and therapeutic margin need to be characterized to demonstrate the feasibility of the local drug therapy. Due to the novelty of our approach, such information is not available in the literature. Medical imaging is one tool that can be used for the *in vivo* assessment of the characteristics of these drug delivery systems. Some current imaging techniques, such as nuclear imaging and magnetic resonance imaging (MRI), are not adequate in resolution or sensitivity, respectively, to provide the necessary pharmacokinetic information [6]. Gamma imaging and positron emission tomography (PET) are the most sensitive noninvasive measurement techniques available for the measurement of radiolabeled drugs at their therapeutic concentrations. However, the drawback of these methods is their low spatial resolution – for example, clinical gamma imaging and PET instruments can only resolve 5 and 10 mm, respectively [7]. Resolutions this low are not adequate to provide an accurate assessment of the pharmacokinetics or the therapeutic margin of newly developed drugs. In addition, since many of the radioisotopes in nuclear imaging studies have relatively short half-lives, they are not suitable for controlled release applications where drug concentrations need to be monitored over a week or more. MRI is another noninvasive technique used to study *in situ* pharmacokinetics [8], having been used in studies of 5-fluorouracil (^{19}F) [9], ^{13}C-labeled temozolomide and ifosfamide (^{31}P) [8]. Although clinical MRI instruments can achieve better spatial resolution ($\sim$ 1 mm) than

Manuscript received November 1, 2001; revised August 13, 2002. The work of K. A. Salem was supported by a Whitaker Fellowship. The work of J. Gao was supported by the NIH under Grant R21-CA093993-01. The work of D. L. Wilson was supported by the NIH under Grant RO1-CA84433-01. *Asterisk indicates corresponding author.*

K. A. Salem was with the Department of Biomedical Engineering, Case Western Reserve University, Cleveland, OH 44106 USA. He is now with Siemens Medical Solutions, Inc., Atlanta, GA, 30322 USA.

A. Szymanski-Exner and M. S. Breen are with the Department of Biomedical Engineering, Case Western Reserve Unversity, Cleveland, OH 44106 USA.

R. S. Lazebnik is with the Department of Biomedical Engineering and the School of Medicine, Case Western Reserve Unversity, Cleveland, OH 44106 USA.

J. Gao is with the Departments of Biomedical Engineering and Radiology, Case Western Reserve Unversity, Cleveland, OH 44106 USA.

*D. L. Wilson is with the Departments of Biomedical Engineering and Radiology, Case Western Reserve Unversity, 10900 Euclid Ave., Cleveland, OH 44106 USA (e-mail: dlw@cwru.edu).

Digital Object Identifier 10.1109/TMI.2002.806270

PET, their main limitation is low sensitivity, making it difficult to detect drugs at their therapeutic concentrations [8].

In comparison, X-ray CT combines excellent spatial resolution with sufficient sensitivity to analyze the pharmacokinetic properties of novel drug delivery systems. CT systems can typically provide submillimeter spatial resolution combined with high temporal resolution. Therefore, tumors on the order of 1 cm in diameter are sufficiently sampled to provide accurate spatial information about platinated drug distribution. Additionally, because a full 3D CT analysis can be performed in less than 1 min, the dynamics of the drug distribution can be followed at different time points. At typical X-ray tube voltages, the X-ray absorption characteristics of platinum give excellent image contrast and sensitivity for *in vivo* drug concentration measurements.

In this report, we develop and demonstrate the effectiveness of image analysis techniques for the *in vivo* evaluation of the pharmacokinetics of platinated drugs from an implanted delivery device using X-ray CT. We first correlate CT signal with local carboplatin concentration, and then use three-dimensional (3-D) visualization as a tool to qualitatively examine the implant with respect to its surrounding anatomy. The use of registration and reformatting allows the straightforward, direct comparison of images acquired at different times. We then use a number of image analysis techniques to quantify the pharmacokinetics of carboplatin release and distribution *in vivo*. As an example application, we compare the *in vivo* release kinetics of carboplatin in normal versus ablated tissue.

II. Methods

A. Calibration of CT Intensity to Drug Concentration

A calibration curve was established for the correlation of CT intensity in Hounsfield units (HUs) to the concentration of carboplatin, an anticancer agent containing platinum, suspended in various gelatin imaging phantoms. The gels were prepared by dissolving carboplatin powder in distilled water at concentrations of 0.0, 0.5, 1.0, 2.5, and 5.0 mg/mL (0.0, 1.35, 2.70, 6.75, and 13.50×10^{-3} mol/L) and adding gelatin powder (10% wet weight) to the heated solution. The solutions were cooled in 12-well polystyrene tissue culture plates for imaging and analysis. CT images of the gels were acquired at 600 mAs, 120 KVp, 1-mm slice thickness and 1.5-second rotation time. To determine the CT intensity for each carboplatin concentration, a 100 voxel cylindrical volume of interest (VOI) was manually defined extending through the four central slices in each of 20 samples (five concentrations with four replicates). The average HU value in the VOI was calculated using ImageJ (Research Services Branch, National Institute of Mental Health, Bethesda, MD), and plotted against carboplatin concentration. Linear regression was used to determine the parameters of a linear fit.

B. Fabrication, Implantation, and Imaging of Drug Delivery Device

Polymer millirods were fabricated according to a previously established heat compression molding procedure [10]. Briefly, poly-lactic-co-glycolic acid (PLGA) microspheres were mixed with carboplatin powder and D(+)-glucose (added to expedite the rate of release). The mixture was placed in a Teflon tube (ID 1.6 mm), inserted into a stainless steel mold and compressed with a 860 g weight at 90°C for 2 h. The resulting cylindrical rod (diameter: 1.6 mm) was cooled to room temperature and removed from the tubing. The resulting implants had a loading density of 10% carboplatin, 40% glucose and 50% PLGA.

Using an Institutional Animal Care and Use Committee approved animal protocol, a male New Zealand white rabbit (3.3 kg) was anesthetized, and the liver was exposed through an incision in the midsection. A small portion of the medial lobe of the liver was ablated with a 19-gauge radio-frequency needle electrode (Radionics, Burlington, MA), at 90 ± 3°C for 3 min. A segment (0.8 cm in length) of the carboplatin millirod implant was then inserted into the ablated lobe. Another identical implant was inserted into normal liver tissue in the right lobe and an external millirod was placed next to the rabbit as a control. To monitor the release of drug from each of the implanted millirods, the rabbit was imaged with an X-ray CT system (Marconi, Mx8000, Cleveland, OH). The rabbit was positioned in the scanner so that the image plane was approximately perpendicular to the long axis of the millirod. The same position was maintained throughout the study and recreated as closely as possible at the different imaging sessions. CT data were acquired with the following settings: spiral scan, 120 kVp, high resolution, B filter, 4×1 collimation, 1.5 s/rotation, 0.5 pitch, and 1.3 mm effective slice thickness. Under these conditions, the maximum current-time allowed by the scanner is 965 mAs. Images were reconstructed using the on-board filtered backprojection algorithm. The first image series was taken at 1 hour following implantation. Subsequent time points were 4 and 24 h following implantation.

C. Registration and Reformatting of CT Volumes

We utilized a 3-D registration method to spatially align the sequence of temporal CT volumes in order to spatially examine drug distributions at different times. The method used line paths, and optional point landmarks, to obtain volume registration [11]. First, we manually localized the intersection of the two cylindrical millirods with every applicable slice. We took care to mark the center of the millirod cross section and calculated the long axis of the rod from the selected center points. Next, we computed an optimum set of rigid body registration parameters by iterative minimization of an objective function representing the mean Euclidean distance between automatically generated correspondence points along the millirod paths. The objective function value, after optimization, provided an estimate of registration error in the region of interest. In addition, based on phantom simulations of manual localization error and millirod orientation, typical of our *in vivo* experiments, we predicted a voxel displacement registration error of approximately $<$ 0.5 mm [11]. Finally, all volumes were transformed so that the millirod was perpendicular to the slice plane, with voxels at the original in-plane resolution of 0.3125 mm and through-plane resolution of 1.3 mm.

D. Evaluation of Drug Pharmacokinetics

Image analysis techniques were used to evaluate the pharmacokinetics of carboplatin release from the implanted millirods.

As described below, processing included background subtraction, circumferential averaging, and regional distribution analysis. In addition, various visualization techniques such as 3-D rendering and surface plots of drug concentration were used.

1) Background Subtraction: To quantitatively evaluate the release of carboplatin from the millirod, the image background was subtracted from each image in the volume, leaving only signal produced by the presence of carboplatin. For each image, a background subtraction mask consisting of three manually segmented regions (millirod, ablated tissue, and normal tissue) was created. For each region, a constant value, corresponding to a previously determined mean value for that region, was calculated from previous studies. In these studies, the value for normal tissue was determined by manually selecting a region of liver background tissue and calculating the mean and standard deviation of the pixel gray levels using ImageJ. The statistics for ablated tissue regions and the empty polymer millirod were measured in a similar fashion. Local signal variation for each tissue type was on the order 2–3 HUs, permitting the use of a constant mean value. Ablation and millirod boundaries were defined for each registered image set to create the subtraction mask. The resulting image was qualitatively examined to verify the subtraction.

2) Circumferentially Averaged Radial Plots: An averaging algorithm was created to evaluate drug transport out of the millirod and into the surrounding tissue. The registration and reformatting process provides a series of axial slices through each millirod, and the subtraction process resulted in images where the entire signal is produced by the presence of carboplatin. The maximum pixel in the ROI surrounding each rod was defined as that rod's center. From this center point, a series of 360 equally spaced radial lines were drawn extending 6.25 mm away from the rod. From the three dimensional data set, the radial profiles of all 360 lines in the three central slices of each registered millirod volume were averaged together. The previously determined relationship between CT signal and drug concentration was then applied to the average profile, converting the CT intensity in HU to the number of drug molecules present in each pixel over time, revealing the release and distribution of carboplatin out of the millirod.

3) Regional Drug Distribution Through a Pillbox Analysis: We examined the local distribution of carboplatin by calculating the number of drug molecules present in a series of virtual "pillboxes." A pillbox is a cylindrical volume defined to enclose a relevant structure such as the millirod or a tumor. In our analysis, we defined three pillboxes: millirod (0–0.8 mm), virtual tumor (0.8–5.0 mm), and surrounding tissue (5.0–6.25 mm). To determine the number of drug molecules in a particular volume of interest (VOI), we integrate over the pillbox and subtract the number of molecules that can be committed to other enclosed regions. For example, the number of molecules in the tumor is equal to the integral over the tumor pillbox minus the integral over the millirod pillbox. The initial number of molecules at the time of implantation (9–10×10^{16} molecules) was determined by measuring a control rod placed outside the rabbit. We assume that the tumor and tissue pillboxes contain no drug when the implant is first introduced. From image data, we counted the number of drug molecules in each of the nearly 1000 voxels within the central 6.25 mm of three 3 central slices of the implants and calculated the amount of drug in each pillbox at 1, 4, and 24 h. A fourth compartment, drug washout, equaled the total drug dosage minus the total number of drug molecules that can be counted in the image. Because the cells in the liver cannot affect the platinum atoms that are retained in the tissue, drug washout provided a measure of vascular clearance as a result of blood perfusion.

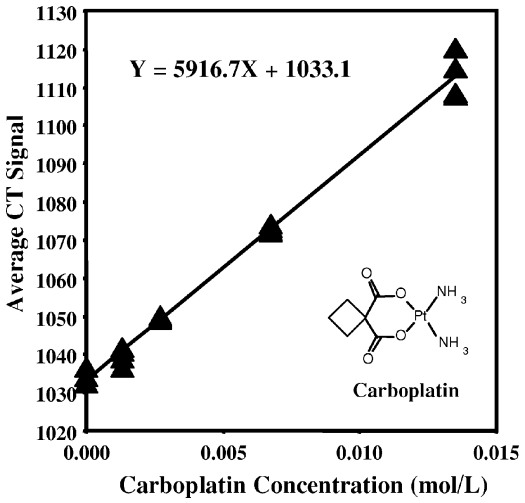

Fig. 1. Carboplatin concentration is linearly correlated with the CT signal. Four data samples from different images were acquired for five different concentrations of carboplatin. The data show a linear correlation between HUs and moles per liter that can be fit by the equation, $Y = 5916.7X + 1033.1$, and the R^2 value of the linear fit is 0.9913.

III. Results

A. Calibration of CT Signal With Drug Concentration

Carboplatin concentration in the gels is plotted against the measured CT signal in Fig. 1. Linear regression resulted in a statistically significant fit ($p < 0.05$) with a slope of 15.97 HU/(mg/mL) and an intercept of 1033.1 HU, the CT signal expected from a gel containing no drug. This corresponds to a sensitivity of 1 HU of CT signal for every 62.6 μg/mL increase in drug concentration. By converting the drug concentration from mg/mL to mol/L, the slope of the linear fit is changed to 5916.7 HU/(mol/L).

B. 3-D Visualization

To visualize the location of the millirods, we created a 3-D reconstruction of the rabbit's torso with a cutout clearly showing the location of the millirods relative to the gall bladder and liver surface (Fig. 2). The image volume consists of $512 \times 512 \times 37$ voxels over a $203 \times 203 \times 119$ mm^3 FOV interpolated to provide isotropic 0.4 mm voxels. The overlay of the liver border shows the near proximity of the millirods to the liver surface. Also, an overlay of the thermal lesion border shows the extent of the lesion and the accurate placement of the millirod at its center.

C. Registration and Reformatting of CT Volumes

Image volumes from the three time points were registered to allow accurate comparison between image sets. In Fig. 3, a vi-

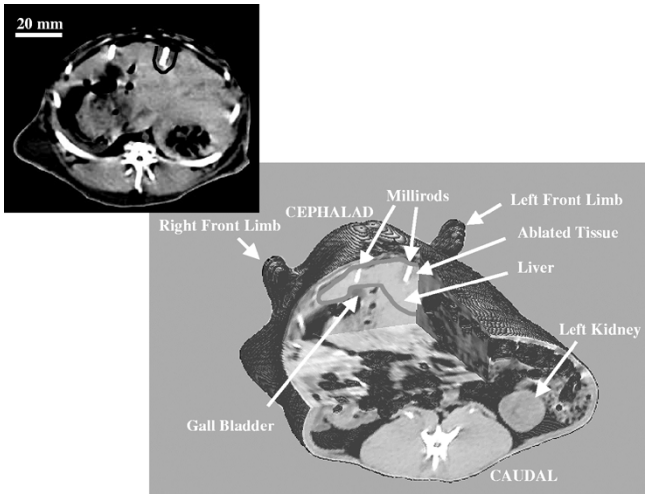

Fig. 2. 3-D rendering of the rabbit's torso and two millirods. A cutout shows the longitudinal cross-section of the two millirods inserted into the liver. The inset shows the CT image corresponding to the plane at the cutout. One millirod was inserted in normal tissue in the liver's right lobe, above the gall bladder. The other millirod was positioned in ablated tissue in the medial lobe of the liver. The thermal lesion is visible as a darkened region surrounding the millirod. The lengths of the millirods appear slightly different since they are not exactly in the same imaging plane.

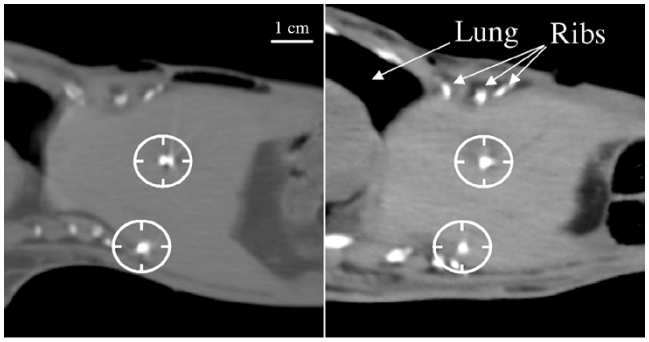

Fig. 3. Registration quality for an *in vivo* rabbit specimen at (a) 4 h and (b) 24 h, post ablation. Registration was performed using the paths of both millirods. The circles were drawn to encompass millirod locations in the right image, and copied to the left image to demonstrate that millirods were well registered. Similar results were seen in image slices throughout the length of the millirod indicating good registration in 3-D.

sual comparison of registered images confirms that the millirod centers are spatially well aligned. The millirod is oriented perpendicular to the image plane, as shown by the circularly symmetric images of the millirod and drug signal. In each of the three imaging sessions, the live rabbit was manually positioned within the gantry; thus, motion of anatomical landmarks, such as the ribs and the diaphragm, between image volumes was expected. Because drug was constrained to only a small portion of the image, the registration process used the millirods. Thus, although some variation in the location of surrounding anatomy is obtained, regions near the millirods should be very well aligned.

D. Evaluation of Drug Pharmacokinetics

In order to perform quantitative evaluation of carboplatin transport, it was necessary to subtract the background leaving only the CT signal from the presence of carboplatin. As

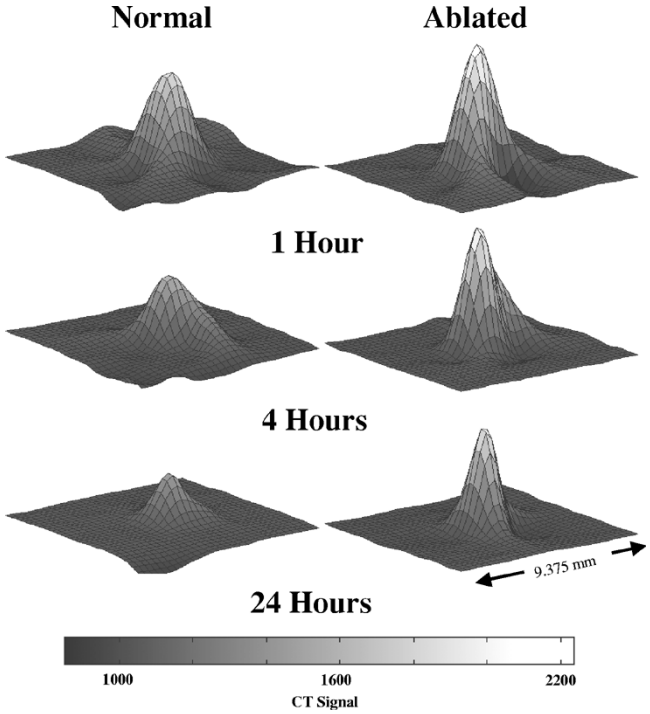

Fig. 4. Surface plots of the signal produced by the implanted millirod and surrounding tissue showing the distribution of drug at 1, 4, and 24 h in both normal (left) and ablated (right) tissue. These results show the raw CT signal, in Hounsfield units, directly as it is received from the imager. In the ablated tissue, the drug release is significantly slower than in normal tissue.

described previously, two-dimensional (2-D) spatial masks were constructed from averages of the CT signal from many slice images. Values are: carboplatin-free polymer rods (858.4 ± 1.06 HU where the latter number is the standard error), liver background (1077.1 ± 0.12 HU), and, when necessary, ablated tissue (1054 ± 0.64 HU). These numbers were consistent over multiple rabbits, multiple imaging sessions, and multiple samples from each session.

1) Visualization of Drug Transport: The transport of carboplatin from the implanted millirods into the surrounding tissues was evaluated by examining surface plots showing the extent of drug penetration (Fig. 4). Plots were created from the central slice in each of the six volumes consisting of normal and ablated tissue at each of the three time points, 1, 4, and 24 h. The peak signal, located at the center of each plot, decreases with time showing continual loss of drug from the millirod. The peak signal in the ablated tissue does not decrease as quickly as that in normal tissue, suggesting that thermal ablation of the surrounding tissue decreases the rate of drug transport from the millirod.

Contour plots of central axial slices from each of the six implants show the quality of background subtraction (Fig. 5). The area in the outer portion of each plot is approximately 0, but the apparent drug signal fluctuates around the actual value since the backgrounds in each volume contain inhomogeneities and local background variation. In regions with little to no appreciable drug, these fluctuations can show negative drug concentrations, which should be considered to be approximately zero. There is less variation in the background of contour plots from ablated regions than normal regions. This uniformity in ablated

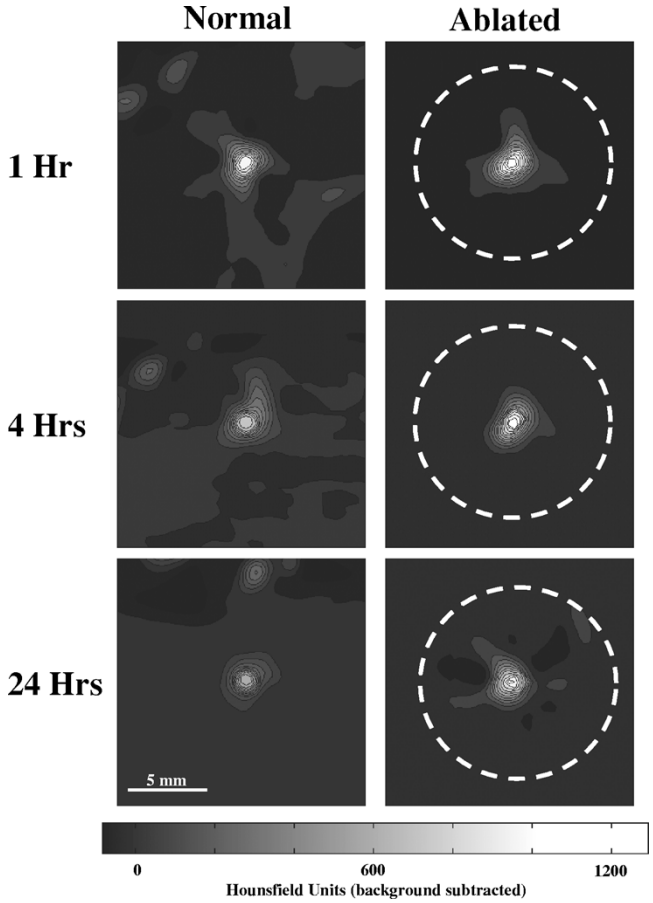

Fig. 5. Contour plots show the spatial distribution of carboplatin in both normal and ablated tissue at 1, 4, and 24 h after subtraction of a background mask. The extent of carboplatin distribution appears to be larger in the ablated tissue at 4 and 24 h, while at 1 h the spread of drug is about the same in both normal and ablated tissue. Because of local inhomogeneity and noise, there are portions of both images that contain negative values.

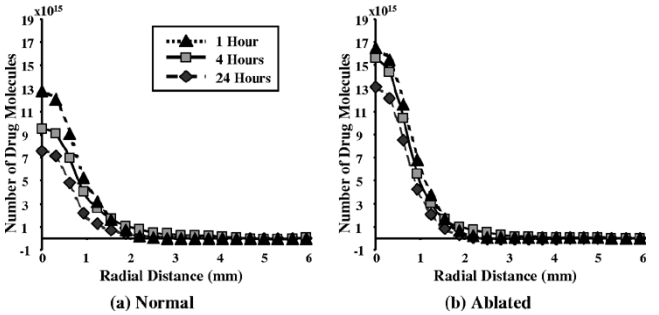

Fig. 6. Radial profiles show the quantitative distribution of carboplatin from the center of the millirod in (a) normal and (b) ablated tissue. The plots show the number of drug molecules as a function of distance from the center of the rod. The amount of drug in the ablated implantation site is much higher than that in the normal site at any two corresponding time points. In each of the six implant conditions, image data were circumferentially averaged across 360 equally spaced radial lines.

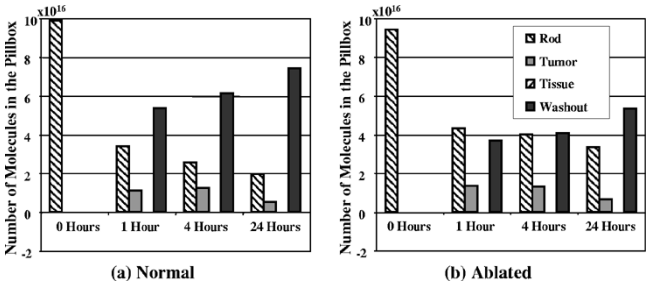

Fig. 7. The pillbox analysis allows one to follow all available drug molecules throughout the course of the experiment. Results from three slices in the center of the millirod are averaged to avoid partial volume effects at the ends of the millirod. The pillboxes are: rod (0–0.8 mm), tumor (0.8–5 mm), and tissue (5–6 mm). Molecules that cannot be accounted for in these regions are assumed to belong to a fourth compartment containing all molecules that were washed out of the local area. The amount of drug in both the rod and tumor is considerably higher in the ablated tissue than in normal tissue.

tissue is likely the result of the destruction of local vasculature. Small blood vessels or bile ducts increase the inhomogeneity of the background making the subtraction of an average gray level more difficult, as seen in the normal tissue.

2) Radial Plots: Figs. 4 and 5 show that drug is transported away from the millirod in all directions. This suggests that an appropriate method for measuring the typical transport is to circumferentially average over a number of radial lines extending from the center of each implant. This averaging shows the distribution of drug as it diffuses into the surrounding tissue and is cleared by the local vasculature (Fig. 6). The normal implants, without ablation, show a rapid decrease in carboplatin both surrounding and inside the rod. Approximately 50% of the drug in the rod is lost between the first hour and the 24th hour. With ablation, however, most of the drug is retained over the same time period. This is most likely the result of the destruction of local vasculature due to the ablation procedure, as supported by histological analysis [12]. In all cases, about 4 mm from the center of the implanted millirod, the CT images no longer show measurable drug concentrations.

3) Pillbox Analysis: The rod (0 – 0.8 mm), virtual tumor (0.8 – 5.0 mm), and surrounding tissue (5.0 – 6.25 mm) pillbox analysis follows all implanted drug molecules as they move through different VOI's during the transport process. Fig. 7 shows the number of molecules in the rod (0–0.8 mm), virtual tumor (0.8—5.0 mm), and surrounding tissue (5.0–6.25 mm), as well as other drug molecules that have been washed out of the region. As shown in the radial plots, the amount of drug inside the rod and in the tumor pillbox is considerably higher in the ablated tissue than in normal tissue, while the tissue pillbox shows no appreciable drug concentration because it is either lower than the sensitivity of the technique or contained within the noise of the liver background. The amount of drug washed out of the treatment site is much higher in normal tissue at all time points, most likely due to the presence of local vasculature. Importantly, the amount of drug inside the rod and tumor pillboxes after 24 h is 25% higher in ablated as opposed to normal tissue.

IV. Discussion

We believe that this work highlights the capabilities of CT as a useful monitoring tool for pharmacokinetic studies. The method is noninvasive, and it can be used to obtain *in vivo* measurements with high spatial resolution at multiple time points in one animal. We were able to achieve high sensitivity (62.6 μg/mL) to the presence of carboplatin in a system that provided in-plane resolution of approximately 0.3 mm. Additionally, because there is a highly linear relationship between gray

level intensity and drug concentration, we can convert image data into quantitative concentration profiles of the distribution of drug molecules. With appropriate image analysis techniques, CT provides both qualitative and quantitative information about the pharmacokinetic behavior of platinated anticancer agents.

The image processing and analysis techniques that we have presented are critical for a full and accurate investigation. The registration and reformatting process is crucial to the accurate analysis of drug pharmacokinetics. Registration allows a number of time points to be compared even though the animal has moved between imaging sessions, while reformatting provides perfect axial slices through the millirod, decreasing partial volume effects and allowing an evaluation of the symmetry of drug transport. We have also presented a number of methods for analyzing the pharmacokinetic behavior of platinated drugs. Visualization, whether in 3-D, through surface plots, or in contour plots, provides important qualitative information about the spatial variation and extent of transport. Accurate background subtraction coupled with circumferential averaging provides previously unknown quantitative information about the concentration of drug at various spatial locations. Finally, our pillbox analysis gives insight into the bulk location of drug at a given time and could easily be expanded to look at the movement of drug to other areas of interest or anatomical locations, such as the kidney or bladder.

A full study of the pharmacokinetic properties of carboplatin should include both CT image data and other more sensitive techniques. The data provided by the CT images allow one implanted millirod to be monitored through a specified time course, decreasing the variability involved in data interpretation. However, the sensitivity of the CT data, $\approx 62\ \mu g/mL$ for each HU, and the background variation, $\approx$ 10 HU standard deviation, limit the ability to reliably measure low carboplatin concentrations. Even with the use of circumferential averaging to decrease the effect of background variation, an independent *t*-test analysis shows that concentrations lower than $\approx 65\ \mu g/mL$ are essentially undetectable with CT (Fig. 6). While much lower than the 200 $\mu g/mL$ plasma concentration applied in systemic drug administration [13], this is still much higher than the cytotoxic concentration of 8–10 $\mu g/mL$ in cell culture experiments [14]. Additionally, while the contrast to noise ratio is an issue with any signal acquisition technique, the averaging that is performed in the analysis techniques helps increase the sensitivity of the system, but not necessarily to a point that can detect the reported therapeutic levels in tissue. More sensitive techniques such as atomic absorption spectrometry [15], [16] and high performance liquid chromatography [15] can measure platinated drug concentration at ng/mL levels and could be used in combination with CT imaging to confirm low-level drug concentration measurements. There are also other techniques that could be used to increase the sensitivity of CT results allowing one to determine the boundary at which a therapeutic dose exists. For example, drug transport models can be used to fit the data provided by the CT images to predict the location of the therapeutic boundary.

It is understood that there are many potential improvements to our measurement techniques. Blurring can be compensated using the modulation transfer function of the system or reduced by changing the reconstruction filter. Partial volume effects can be minimized using correction methods similar to those used in PET [17]. By changing the X-ray beam quality, one might appreciably increase image contrast from the carboplatin. Increasing the X-ray exposure will decrease the effect of image noise, but possibly at the expense of longer acquisition times that might result in more subject motion. Even without these potential modifications, the sensitivity of CT is sufficiently high to reliably detect carboplatin transport at implanted concentrations. Of the above effects, we think that blurring is most important because our image measurement of the number of drug molecules is lower than measurements calculated from a chemical analysis of another rod. We are currently evaluating the effect of system and motion blurring as well as potential other explanations. Nevertheless, the size of the millirod changes little, and as a first approximation, percent changes in the millirod should be relatively unaffected by blurring.

Newer imaging techniques have recently become available that allow very high resolution imaging such as micro-CT and micro-PET. The superior resolution of these techniques ($\sim$ 10–50 mm for micro-CT and $\sim$ 1 mm for micro-PET) make them well suited for applications such as drug studies that require an analysis over small regions. However, micro-CT systems typically have a small focal spot size and limited X-ray production. Hence, to obtain an equivalent SNR, imaging time must be increased. This would be problematic because of subject motion in our *in vivo* study.

There are a number of observations that can be made about the effect of ablating the surrounding tissue before implanting a drug delivery millirod. The most important physiological change caused by the ablation procedure is the destruction of the vasculature [12]. The effect on drug release kinetics are highlighted in this study. The decrease in blood perfusion slows the clearance of carboplatin and causes more drug to remain in the region of the implant (Fig. 4). At the same time, the destruction of cell boundaries and the decease in drug clearance allows the drug to diffuse more freely throughout the ablated area. This is reflected by an increase in the spatial extent of drug diffusion seen in Fig. 5. Because the ablation destroys cells and, therefore, structure in the region, the background is more uniform, and easier to subtract, than in a normal implant where microvasculature and hepatic structure cause more variation in the liver background (Fig. 5).

Some important quantitative results are available from the analysis of the CT images. Results such as shown in Figs. 6 and 7 provide the quantitative change of drug concentration as a function of space and time. These data permit the description of the concentration-time relationships at different locations in the tissue. As demonstrated in systemic chemotherapy, drug efficacy is directly related to both drug concentration and drug exposure time, and the value of area under the plasma concentration-time curve (AUC) is a major factor in optimizing and evaluating drug dosage regimen [18]. Although the systemic data on carboplatin is available in literature [15], such information is not applicable for local therapy since the drug plasma concentration is far from the same as tissue concentration inside the tumor. Compared to standard clinical pharmacokinetic analysis, the CT method provides a direct and noninvasive measure

of the concentration-time curve at the site of action. In combination with histological analysis, the CT data should allow many exciting studies to correlate local pharmacokinetic data to drug efficacy in tumor tissue and potential hepatic toxicity in healthy liver tissue. These studies should permit the determination of optimal carboplatin concentration-time relationships to maximize tumor death while minimizing undesirable toxic side effects.

This study has been a successful proof-of-concept, showing the effectiveness of CT imaging as a technique to determine drug pharmacokinetics. The example application has demonstrated the ability of CT to generate insightful information for understanding local drug transport *in vivo*. This knowledge will permit rational design of drug delivery systems with optimal drug dosage, release rate, and duration to provide a safe and effective localized drug therapy.

REFERENCES

[1] N. Hussain, "Ligand-mediated tissue specific drug delivery," *Adv.Drug Deliv.Rev.*, vol. 43, pp. 95–100, Sept. 2000.

[2] M. Willis and E. Forssen, "Ligand-targeted liposomes," *Adv. Drug Deliv. Rev.*, vol. 29, pp. 249–271, Feb. 1998.

[3] G. Gregoriadis, "Engineering liposomes for drug delivery: Progress and problems," *Trends Biotechnol.*, vol. 13, pp. 527–537, Dec. 1995.

[4] S. Chandran, A. Roy, and B. Mishra, "Recent trends in drug delivery systems: Liposomal drug delivery system– Preparation and characterization," *Indian J. Exp. Biol.*, vol. 35, pp. 801–809, Aug. 1997.

[5] S. Weinbaum and S. Chien, "Lipid transport aspects of atherogenesis," *J. Biomech. Eng.*, vol. 115, pp. 602–610, Nov. 1993.

[6] M. Singh and V. Waluch, "Physics and instrumentation for imaging in-vivo drug distribution," *Adv. Drug Deliv. Rev.*, vol. 41, pp. 7–20, Mar. 2000.

[7] A. Bhatnagar, R. Hustinx, and A. Alavi, "Nuclear imaging methods for noninvasive drug monitoring," *Adv. Drug Deliv. Rev.*, vol. 41, pp. 41–54, Mar. 2000.

[8] J. R. Griffiths and J. D. Glickson, "Monitoring pharmacokinetics of anticancer drugs: Non-invasive investigation using magnetic resonance spectroscopy," *Adv. Drug Deliv. Rev.*, vol. 41, pp. 75–89, Mar. 2000.

[9] W. Wolf, C. A. Presant, and V. Waluch, "^{19}F-MRS studies of fluorinated drugs in humans," *Adv. Drug Deliv. Rev.*, vol. 41, pp. 55–74, Mar. 2000.

[10] F. Qian, A. Szymanski, and J. Gao, "Fabrication and characterization of controlled release poly(D,L-lactide-co-glycolid) millirods," *J. Biomed. Mater. Res.*, vol. 55, pp. 512–522, 2001.

[11] R. S. Lazebnik, T. L. Lancaster, M. S. Breen, J. S. Lewin, and D. L. Wilson, "Volume registration using needle paths and point landmarks for evaluation of interventional MRI treatments," *IEEE Trans. Med. Imag.*, 2003, to be published.

[12] J. Gao, F. Qian, A. Szymanski, N. Stowe, and J. Haaga, "In vivo comparison of drug distribution dynamics in thermoablated and normal rabbit livers," *J. Biomed. Mater. Res.*, vol. 2001, to be published.

[13] B. A. Chabner, C. J. Allegra, G. A. Curt, and P. Calabresi, "Antineoplastic agents," in *Goodman & Gilman's The Pharmacological Basis of Therapeutics*, J. G. Hardman and L. E. Limbird, Eds. New York: McGraw-Hill, 1996, pp. 1233–1288.

[14] S. Pauser, S. Wagner, M. Lippmann, U. Pohlen, R. Reszka, K. J. Wolf, and G. Berger, "Evaluation of efficient chemoembolization mixtures by magnetic resonance imaging therapy monitoring: An experimental study on the VX2 tumor in the rabbit liver," *Cancer Res.*, vol. 56, pp. 1863–1867, 1996.

[15] S. Duffull and B. Robinson, "Clinical pharmacokinetics and dose optimizatoin of carboplatin," *Clin. Pharm.*, vol. 33, pp. 161–183, 1997.

[16] R. Milacic, M. Cemazar, and G. Sersa, "Determination of platinum in tumor tissues after cisplatin therapy by electrothermal atmoic adsorption spectrometry," *J. Pharm. Biomed. Anal.*, vol. 16, pp. 343–348, 1997.

[17] O. G. Rousset, Y. Ma, and A. C. Evans, "Correction for partial volume effects in PET: Principle and validation," *J. Nucl. Med.*, vol. 39, pp. 904–911, May 1998.

[18] L. Z. Benet, D. L. Kroetz, and L. B. Sheiner, "Pharmacokinetics: The dynamics of drug absorption, distribution, and elimination," in *Goodman & Gilman's The Pharmacological Basis of Therapeutics*, J. G. Hardman and L. E. Limbird, Eds. New York: McGraw-Hill, 1996, pp. 1233–1288.